Local thermal energy as a structural indicator in glasses

Jacques Zylberg[a,1], Edan Lerner[b,1], Yohai Bar-Sinai[a,c], and Eran Bouchbinder[a,2]

[a]Chemical Physics Department, Weizmann Institute of Science, Rehovot 7610001, Israel; [b]Institute for Theoretical Physics, University of Amsterdam, 1098 XH Amsterdam, The Netherlands; and [c]School of Engineering and Applied Sciences, Harvard University, Cambridge, MA 02138

Edited by James S. Langer, University of California, Santa Barbara, CA, and approved May 25, 2017 (received for review March 16, 2017)

Identifying heterogeneous structures in glasses—such as localized soft spots—and understanding structure–dynamics relations in these systems remain major scientific challenges. Here, we derive an exact expression for the local thermal energy of interacting particles (the mean local potential energy change caused by thermal fluctuations) in glassy systems by a systematic low-temperature expansion. We show that the local thermal energy can attain anomalously large values, inversely related to the degree of softness of localized structures in a glass, determined by a coupling between internal stresses—an intrinsic signature of glassy frustration—anharmonicity and low-frequency vibrational modes. These anomalously large values follow a fat-tailed distribution, with a universal exponent related to the recently observed universal ω^4 density of states of quasilocalized low-frequency vibrational modes. When the spatial thermal energy field—a "softness field"—is considered, this power law tail manifests itself by highly localized spots, which are significantly softer than their surroundings. These soft spots are shown to be susceptible to plastic rearrangements under external driving forces, having predictive powers that surpass those of the normal modes-based approach. These results offer a general, system/model-independent, physical/observable-based approach to identify structural properties of quiescent glasses and relate them to glassy dynamics.

glasses | structure–dynamics relations | plasticity | universal statistics

Understanding the glassy state of matter remains one of the greatest challenges in condensed matter physics and materials science (1–5). In large part, the elusive nature of the glassy state is due to the absence of well-established tools and concepts to quantify the disordered structures characterizing glassy materials—in sharp contrast to their ordered crystalline counterparts—and because of the lack of understanding of the relations between glassy structures and dynamics. Over the years, many attempts have been made to identify physical quantities that can indicate underlying local structures within glassy materials (6–9). These indicators include, among others, free volume (10–12), internal stresses (13), local elastic moduli (14), local Debye–Waller factor (15), coarse-grained energy and density (16, 17), locally favored structures (18–20), short- and medium-range order (21–23), and various weighted sums over a system-dependent number of low-frequency normal modes (24–30).

These quantities measure some properties of quiescent glasses evaluated at or in the near vicinity of a mechanically (meta-)stable state of a glass (an inherent structure). Some of these indicators are purely structural in nature (i.e., they are obtained from the knowledge of particle positions alone), whereas others require in addition the knowledge of interparticle interactions. Recently, the local yield stress—the minimal local stress needed to trigger an irreversible plastic rearrangement—has been proposed as a structural indicator (31). It is required, however, to externally drive each local region in a glass to its nonlinear rearrangement threshold and hence, belongs to a different class of structural indicators compared with those previously mentioned. The utility of each of the proposed indicators is usually assessed by looking for correlations between the revealed structures—typically localized soft spots—and glassy dynamics, either thermally activated relaxation in the absence of external driving forces or localized irreversible plastic rearrangements under the application of global driving forces. In fact, a recent study established such structure–dynamics correlations by machine-learning techniques, leaving the precise physical nature of the underlying structural indicator unspecified (32, 33). These machine learning-based structural indicators also belong to a different class of structural indicators, because the training stage of the machine-learning algorithm requires knowledge of the plastic rearrangements themselves.

Some of the previously proposed structural indicators have revealed a certain degree of correlation between identified soft spots and dynamics, providing important evidence that preexisting localized structures in a glass significantly affect its dynamics. However, oftentimes, the physical foundations of the structural indicators remain unclear, and they are sometimes defined algorithmically but are not derived from well-established physical observables. Moreover, their statistical properties are not commonly addressed, the relations between them and other basic physical quantities are not established, and the fundamental reasons for them being particularly sensitive to underlying heterogeneous structures in glasses remain elusive.

Here, we propose a structural indicator of glassy "softness"—the local thermal energy (LTE)—which is a transparent physical observable derived by a systematic low-temperature expansion. We use the exact expression for the LTE of interacting particles to elucidate the underlying physical factors—most notably internal stresses, anharmonicity, and nonlinear coupling to low-frequency vibrational modes—that give rise to significant

Significance

When liquids are cooled sufficiently fast, they fail to crystalize and form disordered solids—glasses. Understanding the physical properties of glasses remains a major challenge, in large part because of the lack of tools to characterize the emerging disordered structures and well-established structure–properties relations. In this work, we propose that fluctuational thermal energy reveals highly localized and soft structures in glasses. We show that the degree of softness of these "soft spots" follows a universal fat-tailed statistical distribution and relate it to the density of noncrystalline vibrational states. The softest spots are shown to predict the loci of irreversible plastic rearrangements in sheared glasses, thus offering a generic structure–properties approach to glassy materials.

Author contributions: E.L., Y.B.-S., and E.B. designed research; J.Z. and E.L. performed research; and J.Z., E.L., Y.B.-S., and E.B. wrote the paper.

The authors declare no conflict of interest.

This article is a PNAS Direct Submission.

[1]J.Z. and E.L. contributed equally to this work.

[2]To whom correspondence should be addressed. Email: eran.bouchbinder@weizmann.ac.il.

This article contains supporting information online at www.pnas.org/lookup/suppl/doi:10.1073/pnas.1704403114/-/DCSupplemental.

spatial heterogeneities of softness. We show that the LTE can attain anomalously large values directly related to particularly soft regions in a glass, which follow a fat-tailed distribution. The power law exponent characterizing this distribution is shown to be universal and directly related to the recently observed universal ω^4 density of states of quasilocalized low-frequency vibrational modes (34, 35), constituting a link to a fundamental universal property of glassy systems. The LTE field, a "softness field," thus exhibits highly localized spots, which are significantly softer than their surroundings. These soft spots are shown to be particularly susceptible to plastic rearrangements when the glass is being driven by external forces, having predictive powers that surpass those of the normal modes-based approach (24–27). As such, they can be identified with the long sought for glassy "flow defects," the so-called shear transformation zones (STZ) (36, 37).

Physical Observables in the Low-Temperature Limit

Our starting point is the idea that the thermal average of local physical observables in a system equilibrated at a low temperature T is expected to be sensitive to the system's underlying structure (38). Therefore, we first aim at deriving an expression for the thermal average of a general physical observable $\mathcal{A}$, $\langle \mathcal{A} \rangle_T$, in the low-temperature limit. The latter is given by $\langle \mathcal{A} \rangle_T = \mathcal{Z}(T)^{-1} \int \mathcal{A}(\boldsymbol{x}) \exp\left(-\mathcal{U}(\boldsymbol{x})/k_B T\right) d\boldsymbol{x}$, where the components of the vector $\boldsymbol{x}$ represent the deviations of the system's degrees of freedom from a (possibly local) minimum of its energy $\mathcal{U}(\boldsymbol{x})$, $\mathcal{Z}(T) = \int \exp\left(-\mathcal{U}(\boldsymbol{x})/k_B T\right) d\boldsymbol{x}$ is the partition function, and k_B is the Boltzmann constant. $\langle \mathcal{A} \rangle_T$ can be systematically expanded to leading order in T, yielding (*SI Appendix*)

$$\frac{\langle \mathcal{A} \rangle_T - \mathcal{A}^{(0)}}{\frac{1}{2} k_B T} \simeq \frac{\partial^2 \mathcal{A}}{\partial \boldsymbol{x} \partial \boldsymbol{x}} : \boldsymbol{\mathcal{M}}^{-1} - \frac{\partial \mathcal{A}}{\partial \boldsymbol{x}} \cdot \boldsymbol{\mathcal{M}}^{-1} \cdot \boldsymbol{\mathcal{U}}''' : \boldsymbol{\mathcal{M}}^{-1}, \quad [1]$$

where $\boldsymbol{\mathcal{M}} \equiv \partial^2 \mathcal{U} / \partial \boldsymbol{x} \partial \boldsymbol{x}$ is the dynamical matrix, $\boldsymbol{\mathcal{U}}''' \equiv \partial^3 \mathcal{U} / \partial \boldsymbol{x} \partial \boldsymbol{x} \partial \boldsymbol{x}$ is a third-order anharmonicity tensor, and $\mathcal{A}^{(0)} \equiv \lim_{T \to 0} \langle \mathcal{A} \rangle_T$. All derivatives are evaluated at the minimum of $\mathcal{U}$ (i.e., at $\boldsymbol{x} = \boldsymbol{0}$). In obtaining Eq. **1**, higher-order terms in T were neglected. In the $T \to 0$ limit, these terms vanish, and the right-hand side (RHS) of Eq. **1** represents an intrinsic property of an inherent structure, independent of temperature.

To gain some understanding of the physics encapsulated in Eq. **1**, let us briefly consider a few physical observables. Consider first the total energy $\mathcal{A} = \mathcal{U}(\boldsymbol{x})$ in the quadratic (harmonic) approximation. In this case, the first (harmonic) term on the RHS of Eq. **1** equals the number of degrees of freedom N, and the second (anharmonic) term vanishes because of mechanical equilibrium, $\partial \mathcal{U} / \partial \boldsymbol{x} = \boldsymbol{0}$. Consequently, we obtain $\langle \mathcal{U} \rangle_T - \mathcal{U}^{(0)} = \frac{1}{2} N k_B T$, which is nothing but the equipartition theorem in the harmonic approximation (39). Consider then a system with energy $\mathcal{U}(X)$ that depends on a single (scalar) macroscopic degree of freedom X, representing changes in its linear dimension relative to a reference stable state $X = 0$. In this case, the first (harmonic) term on the RHS of Eq. **1** vanishes, and we obtain $\langle X \rangle_T \simeq -\frac{1}{2} \mathcal{U}''' (\mathcal{U}'')^{-2} k_B T + \mathcal{O}(T^2)$, where a prime denotes a derivative with respect to X. The latter expression describes linear thermal expansion, which is well-known to be an intrinsically anharmonic physical effect proportional to $\mathcal{U}'''$ (39). These examples both show that Eq. **1** is fully consistent with well-established results (equipartition and thermal expansion) and highlight the anharmonic nature of the second term on the RHS of Eq. **1**.

The examples presented above focused on macroscopic (global) scalar observables. Because our main interest is in spatial heterogeneity, we consider now microscopic (local) observables defined at the particles' level. We thus focus on the microscopic generalization of $\langle X \rangle_T$: the thermal displacement vector $\langle \boldsymbol{x} \rangle_T$, which represents the variation of the mean positions of particles about the equilibrium state after thermal fluctuations are introduced. Using Eq. **1**, the normalized thermal average of $\boldsymbol{x}$ in the $T \to 0$ limit takes the form

$$\boldsymbol{\mathcal{X}} \equiv \lim_{T \to 0} \frac{\langle \boldsymbol{x} \rangle_T}{\frac{1}{2} k_B T} = -\boldsymbol{\mathcal{M}}^{-1} \cdot \boldsymbol{\mathcal{U}}''' : \boldsymbol{\mathcal{M}}^{-1}. \quad [2]$$

Note the analogy between Eq. **2**—which features a quadratic (nonlinear) coupling between the anharmonicity tensor $\boldsymbol{\mathcal{U}}'''$ and the inverse of the dynamical matrix $\boldsymbol{\mathcal{M}}^{-1}$—and the expression given above for $\langle X \rangle_T$. The components of the normalized thermal displacement vector $\mathcal{X}_i$ in Eq. **2** should be distinguished from the local Debye–Waller factor x_i^2 (15), with thermal average according to Eq. **1** that is given by $\langle x_i^2 \rangle_T = (\mathcal{M}^{-1})_{ii} k_B T$ (no summation is implied). Although $\langle x_i^2 \rangle_T$ is completely given by the first term on RHS of Eq. **1**, which involves a single contraction of the inverse of the dynamical matrix $\boldsymbol{\mathcal{M}}^{-1}$, $\mathcal{X}_i$ is completely given by the second term, which involves two contractions with $\boldsymbol{\mathcal{M}}^{-1}$. As will be shown below, this distinction makes a qualitative difference. Moreover, $\mathcal{X}_i$ is directly sensitive to anharmonicity, whereas $\langle x_i^2 \rangle_T$ is independent of it. $\boldsymbol{\mathcal{X}}$, plotted in Fig. 1 for a 2D model glass, is shown to exhibit significant spatial heterogeneity, suggesting that it is particularly sensitive to localized soft structures in glasses.

Local Thermal Energy

The normalized thermal displacement vector $\boldsymbol{\mathcal{X}}$, defined in Eq. **2** and shown to exhibit strong spatial heterogeneity in Fig. 1, contributes to the thermal average of any physical observable $\langle \mathcal{A} \rangle_T$ that features $\partial \mathcal{A} / \partial \boldsymbol{x} \neq \boldsymbol{0}$ at $\boldsymbol{x} = \boldsymbol{0}$. It is important to emphasize the counterintuitive result that, for observables with $\partial \mathcal{A} / \partial \boldsymbol{x} \neq \boldsymbol{0}$, anharmonicity seems to be important at vanishingly small temperatures, independent of how well the harmonic approximation for the energy holds. Thus, on the face of it, the normalized thermal displacements $\boldsymbol{\mathcal{X}}$ could have been a good candidate for an indicator of softness of the underlying structure. However, we aim at proposing an observable that naturally "filters out" the regions of homogeneous, collective translation-like motion exhibited by the thermal displacements, further exposing localized soft structures that exhibit large gradients.

Our goal now is to identify a physical observable $\mathcal{A}$ that can potentially serve as a softness field (i.e., a local scalar that features a nonvanishing first spatial derivative and is particularly sensitive to gradients of $\boldsymbol{\mathcal{X}}$). Inspired by ref. 38, an observable that naturally suggests itself is the local potential energy ε_α, where α represents any pair of interacting particles, and $\mathcal{U} = \sum_\alpha \varepsilon_\alpha$. Using Eqs. **1** and **2**, we then define

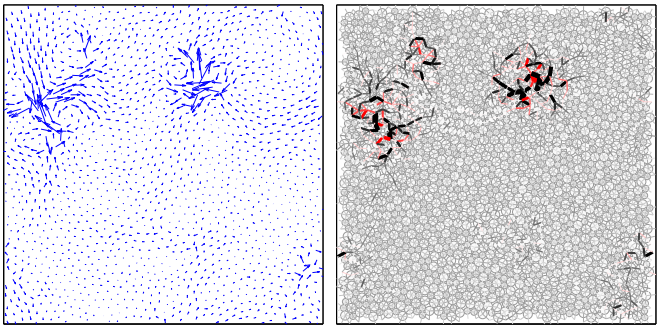

Fig. 1. (*Left*) The normalized thermal displacement vector $\boldsymbol{\mathcal{X}}$, defined in Eq. **2**, measured in a model glass in 2D (details are in the text) of $N = 1{,}600$ particles. (*Right*) A spatial map of the normalized LTE $\mathcal{E}_\alpha$, defined in Eq. **3**, for the same glass realization shown in *Left*. Line thickness and opacity represent the LTE, with red (black) representing negative (positive) LTE.

$$\mathcal{E}_\alpha \equiv \lim_{T\to 0} \frac{\langle \varepsilon_\alpha \rangle_T - \varepsilon_\alpha^{(0)}}{\frac{1}{2} k_B T} = \frac{\partial \boldsymbol{f}_\alpha}{\partial \boldsymbol{x}} : \boldsymbol{\mathcal{M}}^{-1} + \boldsymbol{f}_\alpha \cdot \boldsymbol{\mathcal{X}}, \qquad [3]$$

where $\boldsymbol{f}_\alpha \equiv \partial \varepsilon_\alpha / \partial \boldsymbol{x}$ is the internal force vector acting between particles defining the interaction α.

Mechanical equilibrium at particle i implies that the sum of all of the forces acting on it vanishes. In systems with no internal frustration, internal forces/stresses do not exist, and this sum is trivially satisfied by having $\boldsymbol{f}_\alpha = \boldsymbol{0}$ for all αs. In systems with internal frustration, however, internal forces/stresses generically emerge, $\boldsymbol{f}_\alpha \neq \boldsymbol{0}$. In the former case, the second term on the RHS of Eq. **3** vanishes. Such internal stress-free disordered systems were studied in ref. 38, where it was shown that, under these conditions, $\mathcal{E}_\alpha$ is universally bounded between zero and one. The bound on $\mathcal{E}_\alpha$ suggests that significant spatial heterogeneity in $\mathcal{E}_\alpha$ cannot emerge in internal stress-free systems.

An intrinsic signature of glassy systems is the existence of internal frustration (40) that leads to the emergence of internal forces/stresses, $\boldsymbol{f}_\alpha \neq \boldsymbol{0}$ (1). Consequently, we expect the $\boldsymbol{f}_\alpha \cdot \boldsymbol{\mathcal{X}}$ term on the RHS of Eq. **3** to be generically nonzero for glasses. Because $\boldsymbol{\mathcal{X}}$ is already known to exhibit strongly localized structures, compared with Fig. 1, *Left*, we expect $\boldsymbol{f}_\alpha \cdot \boldsymbol{\mathcal{X}}$ to expose localized regions with a very large concentration of the normalized LTE $\mathcal{E}_\alpha$. In fact, we expect the scalar product of $\boldsymbol{f}_\alpha$ with $\boldsymbol{\mathcal{X}}$ to amplify the spatial heterogeneity in $\boldsymbol{\mathcal{X}}$. To understand this amplification effect, note that $\boldsymbol{f}_\alpha$ is actually a force dipole composed of two forces acting along the line connecting the particles that define the interaction α in opposite directions. Therefore, $\boldsymbol{f}_\alpha \cdot \boldsymbol{\mathcal{X}}$ is exactly the difference between the values of $\boldsymbol{\mathcal{X}}$ at the positions of the particles defining the interaction α, projected along the line connecting them, multiplied by $|\boldsymbol{f}_\alpha|$. Consequently, regions of homogeneous thermal displacements are expected to feature small values of $\boldsymbol{f}_\alpha \cdot \boldsymbol{\mathcal{X}}$, whereas heterogeneous regions—compared with Fig. 1, *Left*—are expected to feature much larger values.

To test these ideas, we plot in Fig. 1, *Right* the normalized LTE $\mathcal{E}_\alpha$ for the same glass realization shown in Fig. 1, *Left*. The result is striking: $\mathcal{E}_\alpha$ attains anomalously large values (both positive and negative) in localized regions where $\boldsymbol{\mathcal{X}}$ exhibits marked heterogeneity. This observation provides strong visual evidence, to be quantified below, that $\mathcal{E}_\alpha$ can be used to define a softness field that clearly identifies localized soft spots in glasses. Finally, note that $\mathcal{E}_\alpha$ can be also measured directly by tracking thermal fluctuations in low T dynamics. Two examples obtained by finite T molecular dynamics (MD) simulations are shown in Fig. 2, *Inset*, showing perfect agreement with the exact expression in Eq. **3**.

Universal Anomalous Statistics

To quantify the degree of softness of soft spots revealed by $\mathcal{E}_\alpha$—compared with Fig. 1, *Right*—and its probability of occurrence, we focus next on the statistical properties of $\mathcal{E}_\alpha$. To this aim, we argue that the statistics of normalized thermal energies $\mathcal{E}_\alpha$ can be related to the density of vibrational frequencies $D(\omega)$. In particular, the form of Eqs. **2** and **3** suggests that soft vibrational modes (i.e., modes with small frequencies ω) give rise to large values of $\mathcal{E}_\alpha$ because of the appearance of the inverse of the dynamical matrix $\boldsymbol{\mathcal{M}}^{-1}$. Recently, it has been observed that low-frequency vibrations in glassy materials appear in two qualitatively different species: one is ordinary long-wavelength plane waves, and the other is disorder-induced soft glassy modes. The former are spatially extended objects, whereas the latter are quasilocalized objects characterized by a disordered core and a power law tail (34). Moreover, long-wavelength plane waves follow a Debye density of states (DOS) $D_D(\omega) \sim \omega^{d-1}$ in d dimensions, whereas soft glassy modes follow a universal DOS $D_G(\omega) \sim \omega^4$ (34, 35). We stress that our focus here is on generic glasses, which do not dwell near a jamming transition, where the physics is expected to change.

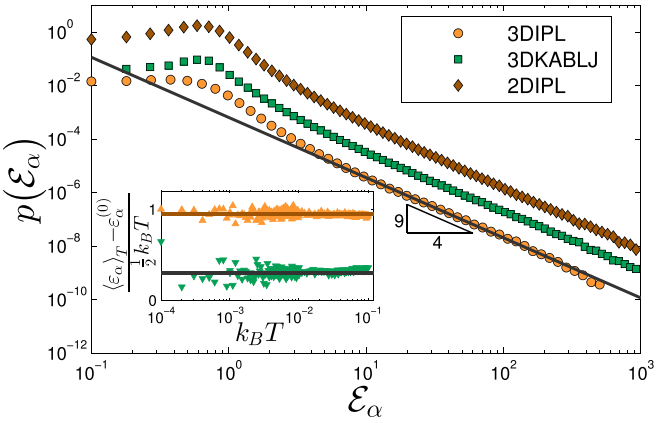

Fig. 2. Distributions of LTE—$p(\mathcal{E}_\alpha)$—measured for three model glasses in 2D and 3D (details are in the text) shifted vertically for visibility. We find a universal form $p(\mathcal{E}_\alpha) \sim \mathcal{E}_\alpha^{-9/4}$ at large LTEs, independent of model or spatial dimension. (*Inset*) MD validation of Eq. **3** for two random interactions in a model glass. The continuous lines represent the exact expression for $\mathcal{E}_\alpha$.

To proceed, note that $\mathcal{E}_\alpha$ in Eq. **3** has one contribution that involves a single contraction with $\boldsymbol{\mathcal{M}}^{-1}$ and another one that involves two contractions with $\boldsymbol{\mathcal{M}}^{-1}$; therefore, the latter is expected to dominate the former. Consequently, we write $\mathcal{E}_\alpha \sim \boldsymbol{f}_\alpha \cdot \boldsymbol{\mathcal{X}}$, with eigen decomposition that takes the form

$$\mathcal{E}_\alpha \sim \sum_{i,j} \frac{(\boldsymbol{f}_\alpha \cdot \boldsymbol{\Psi}_i)\, c_{ijj}}{\omega_i^2\, \omega_j^2} \quad \text{with} \quad c_{ijj} \equiv \boldsymbol{\mathcal{U}}''' : \boldsymbol{\Psi}_i \boldsymbol{\Psi}_j \boldsymbol{\Psi}_j, \qquad [4]$$

where i, j run over all of the vibrational modes $\boldsymbol{\Psi}_i$ defined by the eigenvalue equation $\boldsymbol{\mathcal{M}} \cdot \boldsymbol{\Psi}_i = \omega_i^2 \boldsymbol{\Psi}_i$.

We argue that low-frequency plane waves and quasilocalized soft glassy modes make qualitatively different contributions to the double sum in Eq. **4**. In order to support this claim, we note that, similarly to the discussion about the dipolar nature of $\boldsymbol{f}_\alpha$ above, each contraction of $\boldsymbol{\mathcal{U}}'''$ with a vibrational mode is proportional to the mode's spatial derivative (compare with figure 3 in ref. 41). For low-frequency plane waves, each such derivative is proportional to the frequency ω, whereas for quasilocalized soft glassy modes, the derivative is expected to attain a characteristic value that is nearly independent of frequency. Consequently, because $c_{ijj} \sim \omega^3$ and $\boldsymbol{f}_\alpha \cdot \boldsymbol{\Psi}_i \sim \omega$ for plane waves (which we have numerically verified), we expect their contribution to be negligible compared with that of quasilocalized soft glassy modes, and hence, the above double sum is now understood to be dominated by the latter. Next, because different quasilocalized soft glassy modes are spatially well-separated, we expect c_{ijj} for $i \neq j$ to be much smaller than c_{iii}, such that $\mathcal{E}_\alpha \sim \sum_i (\mathbf{f}_\alpha \cdot \boldsymbol{\Psi}_i)\, c_{iii}\, \omega_i^{-4}$. Finally, because the internal force $\boldsymbol{f}_\alpha$ is localized at the αth interaction, only the glassy mode that is localized there will contribute to the sum, leading to

$$\mathcal{E}_\alpha \sim \omega^{-4}. \qquad [5]$$

Eq. **5**, which is verified below, establishes an important relation between the LTE $\mathcal{E}_\alpha$ and the frequency of vibrational modes ω. In fact, it constitutes a relation between $\mathcal{E}_\alpha$ and the local stiffness $\kappa \equiv \omega^2$, $\mathcal{E}_\alpha \sim \kappa^{-2}$, showing that particularly soft excitations, $\kappa \to 0$, correspond to anomalously large values of the LTE $\mathcal{E}_\alpha$. The predicted relation between local stiffness and LTE justifies the assertion that $\mathcal{E}_\alpha$ quantifies the degree of softness of glassy structures.

Using Eq. **5** and the universal relation $D_G(\omega) \sim \omega^4$, the probability distribution function $p(\mathcal{E}_\alpha)$ is obtained as

$$p(\mathcal{E}_\alpha) = D_G[\omega(\mathcal{E}_\alpha)] \frac{d\omega(\mathcal{E}_\alpha)}{d\mathcal{E}_\alpha} \sim \mathcal{E}_\alpha^{-1} \mathcal{E}_\alpha^{-5/4} \sim \mathcal{E}_\alpha^{-9/4}. \quad [6]$$

Note that, in the above discussion, we implicitly used the fact that the magnitude of the internal forces $|\boldsymbol{f}_\alpha|$ has a characteristic value as shown in *SI Appendix*. The prediction in Eq. **6** has far-reaching implications. First, it suggests that the physical observable $\mathcal{E}_\alpha$ (i.e., the LTE) effectively filters out the effect of low-frequency plane waves, which are known to obscure the origin of many glassy effects (41–43). In fact, when low-frequency plane waves coexist with quasilocalized soft glassy modes in the same frequency range, they hybridize, such that glassy modes acquire spatially extended background displacements and appear to lose their quasilocalized nature. The derivation leading to Eq. **6** assumed that $\mathcal{E}_\alpha$ is insensitive to hybridization and that the $D_G(\omega) \sim \omega^4$ distribution remains physically meaningful (i.e., it still characterizes the probability to find a soft localized structure in a glass) even in the presence of hybridization, when it cannot be directly probed by a harmonic normal modes analysis. Second, the prediction in Eq. **6** rationalizes the existence of anomalously soft localized spots in glassy materials and predicts its probability.

To test the prediction in Eq. **6** and its degree of universality, we performed extensive numerical simulations of different computer glass-forming models [(*i*) a binary system of point-like particles interacting via inverse power law purely repulsive pairwise potentials in 2D (2DIPL) and 3D (3DIPL) (34) and (*ii*) the canonical Kob–Andersen binary Lennard–Jones (3DKABLJ) system (44) in 3D (*SI Appendix* has details about models and methods)] to extract the statistics of $\mathcal{E}_\alpha$ according to Eq. **3**. The results are summarized in Fig. 2. All of the glasses considered exhibit a power law tail with a universal exponent fully consistent with the theoretically predicted $-9/4$ exponent. These results lend strong support to the prediction in Eq. **6** and therefore, also implicitly, its underlying assumptions. The results presented in this section explain the physical origin of the sensitivity of $\mathcal{E}_\alpha$ to soft glassy structures, elucidate its anomalous statistical properties, and establish a relation between its statistical properties and the recently observed universal ω^4 density of states of quasilocalized low-frequency vibrational modes (34), a fundamental property of glasses. Next, we would like to explore the possibility of defining mesoscopic soft spots based on $\mathcal{E}_\alpha$ and their predictive powers.

Softness Field and Predicting Plastic Rearrangements

The normalized LTE $\mathcal{E}_\alpha$ is microscopically defined for any interaction α. In Fig. 3, *Left*, we present yet another example of the spatial map of $\mathcal{E}_\alpha$, here for a larger system compared with Fig. 1, *Right*. A continuous field can be naturally constructed by coarse-graining $|\mathcal{E}_\alpha|$ on a scale larger than the particles scale. We use $|\mathcal{E}_\alpha|$, because anomalously large negative and positive values of $\mathcal{E}_\alpha$ are strongly correlated in space. Coarse-graining is achieved by discretizing space into bins containing at least two bonds each, assigning a bin with softness obtained by averaging the values of $|\mathcal{E}_\alpha|$ of bonds belonging to it, and finally, averaging the bin's value with the values of all bins in the first layer of neighboring bins (*SI Appendix*). Applying this procedure to Fig. 3, *Left* yields Fig. 3, *Right*, which we treat as a softness field. Our goal now is to test the predictive powers of this softness field in relation to glassy dynamics. The latter, either thermally activated relaxation in nondriven conditions or plastic rearrangements under external driving forces, entails crossing some activation barriers. Activation barriers revealed by soft localized vibrational modes $\boldsymbol{\Psi}_i$ of frequency ω_i are small, of order ω_i^6/c_{iii}^2 in the leading anharmonic expansion of the energy (45). Hence, we expect that regions that feature large values of $|\mathcal{E}_\alpha|$ will be particularly susceptible to plastic rearrangements.

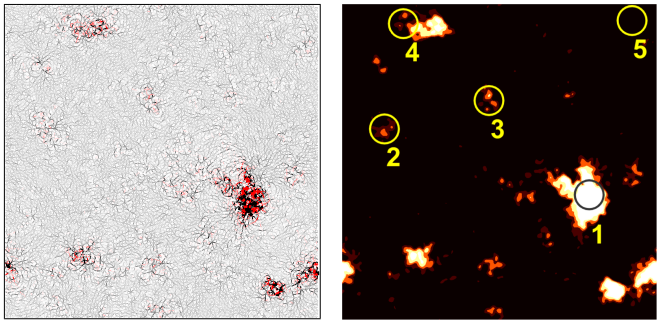

Fig. 3. (*Left*) LTE field in a 2DIPL system of $N = 10{,}000$, same as in Fig. 1. (*Right*) Coarse-grained softness field (in the text). Enumerated by occurrence order are the loci of plastic instabilities that occur upon application of quasistatic shear deformation.

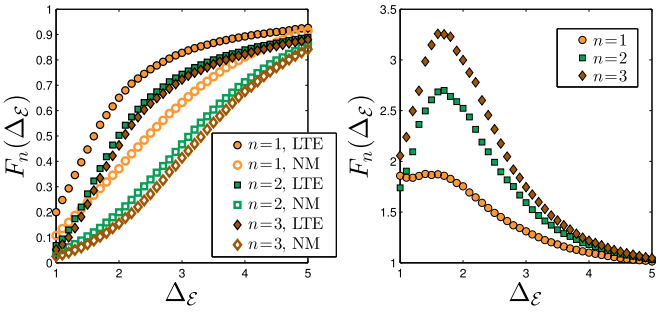

Fig. 4. (*Left*) The cumulative distribution function $F_n(\Delta_\mathcal{E})$ quantifying the fraction of plastic events of ordinal numbers $n = 1, 2, 3$ being closest to soft spots characterized by a value equal to or smaller than $\Delta_\mathcal{E}$ (closed symbols). The corresponding results based on the normal modes (NM) approach (details are in the text) are superimposed (open symbols). (*Right*) The ratio of $F_n(\Delta_\mathcal{E})$ for the two approaches, $\delta F_n(\Delta_\mathcal{E})$, is plotted for $n = 1, 2, 3$. It is clearly observed that the thermal energy-based approach significantly outperforms the NM-based approach.

To test the susceptibility of regions with large LTE to plastic rearrangements, we applied global quasistatic shear deformation in a certain direction under athermal conditions to each glass realization—such as the one shown in Fig. 3, *Right*—and measured the locations of the first few discrete irreversible plastic rearrangements as described in *SI Appendix*. The advantage of this $T = 0$ protocol is that it allows one to uniquely and unquestionably identify the discrete irreversible plastic rearrangements. The locations of the first five discrete irreversible plastic rearrangements (events) were superimposed on the softness field in Fig. 3, *Right*. The first four plastic events overlap soft spots identified by the softness field, indicating a high degree of predictiveness of $\mathcal{E}_\alpha$.

To quantify the degree of predictiveness of the LTE $\mathcal{E}_\alpha$, we extracted the location of soft spots from the spatial distribution of $\mathcal{E}_\alpha$ (for example, the one shown in Fig. 3) as described in *SI Appendix*. In addition to its location, each soft spot is characterized by its degree of softness, representing the average value of $|\mathcal{E}_\alpha|$ in its near vicinity (*SI Appendix*). Because the fat-tailed distribution in Eq. **6** predicts very large variability in the degree of softness of different soft spots within a single glass realization and among different realizations, we define $\Delta_\mathcal{E}$ of each soft spot as the maximal degree of softness in a given realization divided by the spot's degree of softness. That way, we standardize the degree of softness, such that the softest spot in each realization has $\Delta_\mathcal{E} = 1$ and not as soft spots have $\Delta_\mathcal{E} > 1$. Then, each plastic event of ordinal number n ($n = 1$ for the first event, $n = 2$ for the second,

etc.) is associated with the soft spot that is closest to it in space (*SI Appendix*). We stress that the soft spots are extracted for the nonsheared system and are not updated between plastic events.

The cumulative distribution function $F_n(\Delta_\mathcal{E})$, quantifying the fraction of plastic events of ordinal number n being closest to soft spots characterized by a value equal to or smaller than $\Delta_\mathcal{E}$, is constructed by collecting data from 5,000 independent simulations of 2DIPL computer glasses. $F_n(\Delta_\mathcal{E})$ for $n=1,2,3$ is shown in Fig. 4, *Left*, closed symbols. As expected, the smaller the n, the larger the predictive power. Moreover, it is observed that about 20% of the first plastic events (i.e., $n=1$) are predicted by the softest spot in each realization and that nearly 70% are predicted by soft spots with $\Delta_\mathcal{E} \leq 2$. To assess how good these predictive powers are, we need some reference case to compare with, which we consider next.

Among the many structural indicators studied over the years (compare with the Introduction above), the normal modes-based approach (24–27) stands out according to the relatively high correlations between the structure and dynamics that it exhibits. The basic idea behind this approach is that, although a single low-lying normal mode $\mathbf{\Psi}_i$ does not clearly exhibit localized structures, possibly because of hybridization, some weighted sum over a system-dependent number of normal modes does reveal such structures. We use this approach here to compare its predictions with the predictions obtained above based on the LTE. In particular, we follow ref. 15 and construct maps analogous to Fig. 3, *Left* and Fig. 1, *Right* by summing the norm squared of the components of low-lying normal modes $\mathbf{\Psi}_i$ at each particle over the first 30 nonzero modes (i.e., $\sum_{i=1}^{30} |\mathbf{\Psi}_i^{(j)}|^2$) for every particle j. Here, $\mathbf{\Psi}_i^{(j)} \equiv (\Psi_{i,x}^{(j)}, \Psi_{i,y}^{(j)})$ are the components of the normal mode $\mathbf{\Psi}_i$ at particle j, and x, y are the axes directions in a global 2D Cartesian coordinate system.

After the normal modes maps are constructed (*SI Appendix* has more details), we apply to them the same procedure described above and calculate the cumulative distribution function $F_n(\Delta_\mathcal{E})$ based on them. The results are superimposed on the LTE results in Fig. 4, *Left*, open symbols. The comparison reveals that the thermal energy-based approach significantly outperforms the normal modes-based approach. The performance of both approaches is quantified in Fig. 4, *Right*, where we plot the ratio of $F_n(\Delta_\mathcal{E})$ for the two approaches for $n=1,2,3$, $\delta F_n(\Delta_\mathcal{E})$, showing that the thermal energy-based approach outperforms the normal modes-based approach by up to a factor of 1.85 for $n=1$ and up to a factor of 3.3 for $n=3$.

We thus conclude that the LTE has predictive powers that surpass those of the normal modes-based approach. Can we also assess its predictive powers in absolute terms? To address this question, one should note that soft spots are expected to be anisotropic objects (41, 46) characterized by orientation and polarity and hence, feature variable coupling to shearing in various directions. That is, they are expected to be spin-like objects. Consequently, a spot that is very soft in a given direction may not undergo a rearrangement if the projection of the driving force on its soft direction is small. Hence, the optimal predictive power based on the degree of softness alone—a scalar measure—may be significantly smaller than unity. In particular, assuming a uniform/isotropic orientational distribution of equally soft spots, a naive estimation indicates that only 25% of them will rearrange under shearing in a given direction. As a result, the $\sim 20\%$ predictive power of the softest soft in each realization, compared with Fig. 4, *Left*, closed symbols ($n=1$), may, in fact, be not so far from the optimal scalar predictiveness level. The optimal scalar predictiveness issue certainly deserves additional investigation.

Conclusion

We have shown that the low-temperature LTE $\mathcal{E}_\alpha$ is a physical observable that is particularly sensitive to localized soft structures in glasses. $\mathcal{E}_\alpha$ effectively filters out the contribution of long-wavelength plane waves; hence, it is dominated by soft glassy vibrational modes alone. This property allows one to establish a quantitative relation between the recently observed universal distribution of soft glassy vibrational modes, $D_G(\omega) \sim \omega^4$ in the limit of small frequencies ω, and the distribution of the LTE, $p(\mathcal{E}_\alpha) \sim \mathcal{E}_\alpha^{-9/4}$ in the limit of large $\mathcal{E}_\alpha$. This universal anomalous, fat-tailed distribution of $\mathcal{E}_\alpha$ has been supported by extensive simulations on various computer glass-former in 2D and 3D.

Although the problems of coexistence and hybridization of long-wavelength plane waves and soft vibrational modes, which have hampered a direct observation of soft quasilocalized glassy modes and their statistical distribution for a long time, will be addressed elsewhere, we stress that our results have potentially important implications in this context. The universal fat-tailed distribution $p(\mathcal{E}_\alpha) \sim \mathcal{E}_\alpha^{-9/4}$ has been theoretically derived based on the DOS of soft quasilocalized vibrational modes $D_G(\omega) \sim \omega^4$. However, the LTE $\mathcal{E}_\alpha$ is a physical quantity that is defined without any explicit reference to soft quasilocalized vibrational modes or any harmonic normal modes analysis. Consequently, it should be valid in the thermodynamic limit where the harmonic normal modes analysis may not cleanly reveal soft quasilocalized vibrational modes or their ω^4 DOS. As such, it suggests that the ω^4 distribution has a physical meaning that goes beyond the eigenvalues of harmonic normal modes, where $\kappa = \omega^2$ is a generalized measure the stiffness of localized soft glassy structures (43).

The universal anomalous distribution of $\mathcal{E}_\alpha$ and its relation to the universal localized glassy modes DOS imply the existence of highly localized and soft structures in glassy materials. Consequently, $\mathcal{E}_\alpha$ forms a softness field that naturally reveals soft spots. These soft spots are expected to be characterized by particularly small activation barriers and hence, predict the loci of plastic rearrangements under shearing. As such, these soft spots are natural candidates for STZ (36, 37). The predictive powers of the LTE have been substantiated by extensive numerical simulations and have been shown to be superior to those of the normal modes-based structural indicator.

Our approach offers a general system/model-independent, physical/observable-based framework to identify structural properties of quiescent glasses and relate them to glassy dynamics. In particular, the identified field of soft spots and its time evolution under external driving forces should play a major role in theories of plasticity of amorphous materials, serving to define a population of STZ (37, 47–50). The predictive powers of our approach have been shown here for plastic rearrangements in athermal quasistatically driven systems. An important future challenge would be to test whether and to what extent these predictive powers persist at finite temperatures—possibly up to the glass transition region—and finite strain rates. It should also be tested against thermally activated relaxation in the absence of external driving forces. Finally, as mentioned above, an interesting direction would be to go beyond the scalar degree of softness measure by incorporating orientational information into a generalized structural indicator.

1. Alexander S (1998) Amorphous solids: Their structure, lattice dynamics and elasticity. *Phys Rep* 296:65–236.
2. Dyre JC (2006) Colloquium: The glass transition and elastic models of glass-forming liquids. *Rev Mod Phys* 78:953–972.
3. Cavagna A (2009) Supercooled liquids for pedestrians. *Phys Rep* 476:51–124.
4. Berthier L, Biroli G (2011) Theoretical perspective on the glass transition and amorphous materials. *Rev Mod Phys* 83:587–645.
5. Binder K, Kob W (2011) *Glassy Materials and Disordered Solids: An Introduction to Their Statistical Mechanics (Revised Edition)* (World Scientific, Singapore).

6. Hocky GM, Coslovich D, Ikeda A, Reichman DR (2014) Correlation of local order with particle mobility in supercooled liquids is highly system dependent. *Phys Rev Lett* 113:157801.
7. Aharonov E, Bouchbinder E, Hentschel HGE, Ilyin V, Makedonska N, Procaccia I, Schupper N. (2007) Direct identification of the glass transition: Growing length scale and the onset of plasticity. *Europhys Lett* 77:56002.
8. Jack RL, Dunleavy AJ, Royall CP (2014) Information-theoretic measurements of coupling between structure and dynamics in glass formers. *Phys Rev Lett* 113:095703.
9. Royall CP, Williams SR (2015) The role of local structure in dynamical arrest. *Phys Rep* 560:1–75.
10. Spaepen F (1977) A microscopic mechanism for steady state inhomogeneous flow in metallic glasses. *Acta Metall* 25:407–415.
11. Spaepen F (2006) Homogeneous flow of metallic glasses: A free volume perspective. *Scr Mater* 54:363–367.
12. Widmer-Cooper A, Harrowell P (2006) Free volume cannot explain the spatial heterogeneity of Debye–Waller factors in a glass-forming binary alloy. *J Non Cryst Solids* 352:5098–5102.
13. Srolovitz D, Maeda K, Vitek V, Egami T (1981) Structural defects in amorphous solids statistical analysis of a computer model. *Philos Mag A* 44:847–866.
14. Tsamados M, Tanguy A, Goldenberg C, Barrat JL (2009) Local elasticity map and plasticity in a model lennard-jones glass. *Phys Rev E* 80:026112.
15. Widmer-Cooper A, Harrowell P (2006) Predicting the long-time dynamic heterogeneity in a supercooled liquid on the basis of short-time heterogeneities. *Phys Rev Lett* 96:185701.
16. Matharoo GS, Razul MSG, Poole PH (2006) Structural and dynamical heterogeneity in a glass-forming liquid. *Phys Rev E* 74:050502.
17. Berthier L, Jack RL (2007) Structure and dynamics of glass formers: Predictability at large length scales. *Phys Rev E* 76:041509.
18. Coslovich D, Pastore G (2007) Understanding fragility in supercooled lennard-jones mixtures. I. Locally preferred structures. *J Chem Phys* 127:124504.
19. Royall CP, Williams SR, Ohtsuka T, Tanaka H (2008) Direct observation of a local structural mechanism for dynamic arrest. *Nat Mater* 7:556–561.
20. Malins A, Eggers J, Royall CP, Williams SR, Tanaka H (2013) Identification of long-lived clusters and their link to slow dynamics in a model glass former. *J Chem Phys* 138:12A535.
21. Shi Y, Falk ML (2005) Strain localization and percolation of stable structure in amorphous solids. *Phys Rev Lett* 95:095502.
22. Tanaka H (2005) Relationship among glass-forming ability, fragility, and short-range bond ordering of liquids. *J Non Cryst Solids* 351:678–690.
23. Kawasaki T, Araki T, Tanaka H (2007) Correlation between dynamic heterogeneity and medium-range order in two-dimensional glass-forming liquids. *Phys Rev Lett* 99:215701.
24. Widmer-Cooper A, Perry H, Harrowell P, Reichman DR (2008) Irreversible reorganization in a supercooled liquid originates from localized soft modes. *Nat Phys* 4:711–715.
25. Tanguy A, Mantisi B, Tsamados M (2010) Vibrational modes as a predictor for plasticity in a model glass. *Europhys Lett* 90:16004.
26. Manning ML, Liu AJ (2011) Vibrational modes identify soft spots in a sheared disordered packing. *Phys Rev Lett* 107:108302.
27. Rottler J, Schoenholz SS, Liu AJ (2014) Predicting plasticity with soft vibrational modes: From dislocations to glasses. *Phys Rev E* 89:042304.
28. Mosayebi M, Ilg P, Widmer-Cooper A, Del Gado E (2014) Soft modes and nonaffine rearrangements in the inherent structures of supercooled liquids. *Phys Rev Lett* 112:105503.
29. Schoenholz SS, Liu AJ, Riggleman RA, Rottler J (2014) Understanding plastic deformation in thermal glasses from single-soft-spot dynamics. *Phys Rev X* 4:031014.
30. Ding J, Patinet S, Falk ML, Cheng Y, Ma E (2014) Soft spots and their structural signature in a metallic glass. *Proc Natl Acad Sci USA* 111:14052–14056.
31. Patinet S, Vandembroucq D, Falk ML (2016) Connecting local yield stresses with plastic activity in amorphous solids. *Phys Rev Lett* 117:045501.
32. Cubuk ED, Schoenholz SS, Rieser JM, Malone BD, Rottler J, Durian DJ, Kaxiras E, Liu AJ (2015) Identifying structural flow defects in disordered solids using machine-learning methods. *Phys Rev Lett* 114:108001.
33. Schoenholz SS, Cubuk ED, Sussman DM, Kaxiras E, Liu AJ (2016) A structural approach to relaxation in glassy liquids. *Nat Phys* 12:469–471.
34. Lerner E, Düring G, Bouchbinder E (2016) Statistics and properties of low-frequency vibrational modes in structural glasses. *Phys Rev Lett* 117:035501.
35. Mizuno H, Shiba H, Ikeda A (2017) Continuum limit of the vibrational properties of amorphous solids. arXiv:1703.10004.
36. Argon AS (1979) Plastic deformation in metallic glasses. *Acta Metall* 27:47–58.
37. Falk ML, Langer JS (1998) Dynamics of viscoplastic deformation in amorphous solids. *Phys Rev E* 57:7192–7205.
38. Bar-Sinai Y, Bouchbinder E (2015) Spatial distribution of thermal energy in equilibrium. *Phys Rev E* 91:060103.
39. Chaikin PM, Lubensky TC (2000) *Principles of Condensed Matter Physics* (Cambridge Univ Press, Cambridge, UK).
40. Tarjus G, Kivelson SA, Nussinov Z, Viot P (2005) The frustration-based approach of supercooled liquids and the glass transition: A review and critical assessment. *J Phys Condens Matter* 17:R1143–R1182.
41. Lerner E (2016) Micromechanics of nonlinear plastic modes. *Phys Rev E* 93:053004.
42. Wijtmans S, Manning ML (2015) Disentangling defects and sound modes in disordered solids. arXiv:1502.00685.
43. Gartner L, Lerner E (2016) Nonlinear modes disentangle glassy and Goldstone modes in structural glasses. *SciPost Phys* 1:016.
44. Kob W, Andersen HC (1995) Testing mode-coupling theory for a supercooled binary lennard-jones mixture I: The van hove correlation function. *Phys Rev E* 51:4626–4641.
45. Gartner L, Lerner E (2016) Nonlinear plastic modes in disordered solids. *Phys Rev E* 93:011001.
46. Maloney CE, Lemaître A (2006) Amorphous systems in athermal, quasistatic shear. *Phys Rev E* 74:016118.
47. Bouchbinder E, Langer JS, Procaccia I (2007) Athermal shear-transformation-zone theory of amorphous plastic deformation. I. Basic principles. *Phys Rev E* 75:036107.
48. Bouchbinder E, Langer JS (2009) Nonequilibrium thermodynamics of driven amorphous materials. III. Shear-atransformation-zone plasticity. *Phys Rev E* 80:031133.
49. Bouchbinder E, Langer JS (2011) Linear response theory for hard and soft glassy materials. *Phys Rev Lett* 106:148301.
50. Falk ML, Langer JS (2011) Deformation and failure of amorphous, solidlike materials. *Annu Rev Condens Matter Phys* 2:353–373.

SUPPORTING INFORMATION

This Supporting Information is organized as follows: in Section **A** we provide details about the glass-forming models we employed in this work, and the preparation protocol used to generate our ensemble of glassy samples. In Section **B** the first-order expansion in temperature of an interaction energy is derived, from which the definition of a LTE $\mathcal{E}_\alpha$ emerges. We further explain how we calculate LTEs numerically, and discuss the generality of our results. In Section **C** we present distributions of the magnitude of forces between particles in our model glass. In Section **D** we describe how the LTE field is processed to give rise to soft spots and to predictions of ensuing plastic instabilities under shear. In Section **E** we explain how we quantify the level of predictiveness of the LTE field and describe how soft spot maps based on a normal-mode analysis are constructed.

A. MODELS AND PREPARATION PROTOCOLS

Models — We employ a single glass-forming model in two-dimensions (2D), and two glass-forming models in 3D, referred to as the 2DIPL, 3DIPL, and 3DKABLJ systems, respectively. The 2DIPL model is a 50:50 binary mixture of 'large' and 'small' particles of equal mass m, interacting via radially-symmetric purely repulsive inverse power-law pairwise potentials, that follow

$$\varphi(r_{ij}) = \begin{cases} \epsilon\left[\left(\frac{\lambda_{ij}}{r_{ij}}\right)^n + \sum_{\ell=0}^{q} c_{2\ell}\left(\frac{r_{ij}}{\lambda_{ij}}\right)^{2\ell}\right] & , \ \frac{r_{ij}}{\lambda_{ij}} \le x_c \\ 0 & , \ \frac{r_{ij}}{\lambda_{ij}} > x_c \end{cases}, \tag{A.1}$$

where r_{ij} is the distance between the i^{th} and j^{th} particles, ϵ is an energy scale, and x_c is the dimensionless distance for which φ_{IPL} vanishes continuously up to q derivatives. Distances are measured in terms of the interaction lengthscale λ between two 'small' particles, and the rest are chosen to be $\lambda_{ij}=1.18\lambda$ for one 'small' and one 'large' particle, and $\lambda_{ij}=1.4\lambda$ for two 'large' particles. The coefficients $c_{2\ell}$ are given by

$$c_{2\ell} = \frac{(-1)^{\ell+1}}{(2q-2\ell)!!(2\ell)!!}\frac{(n+2q)!!}{(n-2)!!(n+2\ell)}x_c^{-(n+2\ell)}. \tag{A.2}$$

We chose the parameters $x_c=1.48$, $n=10$, and $q=3$. The density was set to be $N/V=0.86\lambda^{-2}$; this choice sets the scale of characteristic $T=0$ interaction energies to be of order unity. We emphasize that this model glass-former does not lie in the proximity of an unjamming point since it possesses an intrinsic invariance to variations of density (or pressure), as established by the extensive work of Dyre et al. [1–3]. Indeed, none of the observables measured in our simulations or in our analysis depend on our particular choice of density. The 2DIPL model undergoes a computer-glass-transition at a temperature of $T_g \approx 0.5\epsilon/k_B$ for the density we chose.

The 3DIPL model is the three-dimensional version of the 2DIPL. Here we follow the same reasoning in setting the density and choose $N/V=0.82\lambda^{-3}$. The resulting glass transition temperature is $T_g \approx 0.52\epsilon/k_B$.

The 3DKABLJ is the canonical Kob-Andersen binary Lennard-Jones model [4]. It is a binary mixture of 80% type A particles and 20% type B particles of equal mass m, interacting via the following radially-symmetric pairwise potential

$$\varphi(r_{ij}) = \begin{cases} \varphi_{\text{LJ}}\left(\frac{r_{ij}}{\lambda_{ij}}\right) + \epsilon_{ij}\sum_{\ell=0}^{3} c_{2\ell}\left(\frac{r_{ij}}{\lambda_{ij}}\right)^{2\ell} & , \ \frac{r_{ij}}{\lambda_{ij}} \le x_c \\ 0 & , \ \frac{r_{ij}}{\lambda_{ij}} > x_c \end{cases}, \tag{A.3}$$

where $\varphi_{\text{LJ}}\left(\frac{r_{ij}}{\lambda_{ij}}\right) = 4\epsilon_{ij}\left[\left(\frac{r_{ij}}{\lambda_{ij}}\right)^{12} - \left(\frac{\lambda_{ij}}{r_{ij}}\right)^{6}\right]$ is the conventional Lennard-Jones potential. Energies are expressed in terms of the A-A interaction $\epsilon \equiv \epsilon_{AA}$, then $\epsilon_{AB}=1.5\epsilon$ and $\epsilon_{BB}=0.5\epsilon$. The interaction length parameters are expressed in terms of $\lambda \equiv \lambda_{AA}$, then $\lambda_{AB}=0.8$ and $\lambda_{BB}=0.88$. $x_c=2.5$ is the dimensionless distance for which φ vanishes continuously up to three derivatives. This condition sets the values of the coefficients $c_0=0.322042855424$, $c_2=-0.11564551766016$, $c_4=0.014774794872422$ and $c_4=-0.0006556954772111$. The density was set at $N/V=1.2$. With this parameter set the system undergoes a computer glass transition at $T_g \approx 0.45\epsilon/k_B$.

Preparation protocol — We prepared ensembles of glassy samples for all three models using the following protocol: first, systems were equilibrated in the high temperature liquid phase at $T=1.0\epsilon/k_B$. Then, the temperature was instantaneously set to a target value just below the respective T_g of each model, where the dynamics were ran for a duration $t_{\text{anneal}}=200\tau_0, 250\tau_0$ and $50\tau_0$ for the 2DIPL, 3DIPL and 3DKABLJ, respectively. Here $\tau_0 \equiv \sqrt{m}\lambda/\epsilon$ is the microscopic units of time. This short annealing step is necessary to avoid generating unphysical ultra-unstable glassy configurations that could occur in an instantaneous quench, and is computationally advantageous compared to a continuous quench at a fixed quench-rate. After the annealing step we minimized the energy to produce glassy samples by a standard conjugate gradient method. Using this protocol, we have generated 5000 independent glassy samples for all three models, with $N=10000$ for the 2DIPL system, and $N=2000$ for the 3DIPL and 3DKABLJ systems.

B. LOCAL THERMAL ENERGIES

In most of our work we omit particle indices with the goal of improving the clarity and readability of the text. We denote Nd-dimensional vectors as $\boldsymbol{v}$, each component

pertains to some particle index (e.g. i) and some Cartesian spatial component (e.g. ξ). Single, double and and triple contractions are denoted with $\cdot,:$, and $\vdots$, respectively. For example, the notation $\frac{\partial^3\mathcal{A}}{\partial\boldsymbol{x}\partial\boldsymbol{x}\partial\boldsymbol{x}}\vdots\boldsymbol{x}\boldsymbol{x}\boldsymbol{x}$ should be interpreted as $\sum_{ijk\xi\nu\upsilon}\frac{\partial^3\mathcal{A}}{\partial x_{i\xi}\partial x_{j\nu}\partial x_{k\upsilon}}x_{i\xi}x_{j\nu}x_{k\upsilon}$, where i,j,k run over particle indices and ξ,ν,υ run over Cartesian spatial components.

We begin with deriving an expression for the thermal average of a general observable $\mathcal{A}=\mathcal{A}(\boldsymbol{x})$ which depends on the coordinates $\boldsymbol{x}$, defined here as the displacement about an inherent state configuration. We denote with the superscript '(0)' quantities evaluated at the inherent state $\boldsymbol{x}=0$ (i.e. at zero temperature), e.g. $\mathcal{A}^{(0)}$, and $\mathcal{U}(\boldsymbol{x})$ denotes the potential energy.

The mean of the observable $\mathcal{A}$ is a function of temperature, defined as

$$\langle\mathcal{A}\rangle_{_T}\equiv\frac{\int\mathcal{A}(\boldsymbol{x})\exp\left(-\frac{\mathcal{U}(\boldsymbol{x})}{k_BT}\right)d\boldsymbol{x}}{\int\exp\left(-\frac{\mathcal{U}(\boldsymbol{x})}{k_BT}\right)d\boldsymbol{x}}=\frac{\int\mathcal{A}(\boldsymbol{x})\exp\left(-\frac{\delta\mathcal{U}(\boldsymbol{x})}{k_BT}\right)d\boldsymbol{x}}{\tilde{\mathcal{Z}}(T)}\,, \tag{B.1}$$

where $\delta\mathcal{U}\equiv\mathcal{U}-\mathcal{U}^{(0)}$ is the energy variation about the inherent state energy $\mathcal{U}^{(0)}$, and $\tilde{\mathcal{Z}}(T)\equiv\int\exp\left(-\frac{\delta\mathcal{U}(\boldsymbol{x})}{k_BT}\right)d\boldsymbol{x}$ is the relevant partition function. $\delta\mathcal{U}$ is expanded to third order in the coordinates as

$$\delta\mathcal{U}\simeq\tfrac{1}{2}\boldsymbol{\mathcal{M}}:\boldsymbol{x}\boldsymbol{x}+\tfrac{1}{6}\boldsymbol{\mathcal{U}}'''\vdots\boldsymbol{x}\boldsymbol{x}\boldsymbol{x}\,, \tag{B.2}$$

where $\boldsymbol{\mathcal{M}}\equiv\frac{\partial^2\mathcal{U}}{\partial\boldsymbol{x}\partial\boldsymbol{x}}$ is the dynamical matrix, and $\boldsymbol{\mathcal{U}}'''\equiv\frac{\partial^3\mathcal{U}}{\partial\boldsymbol{x}\partial\boldsymbol{x}\partial\boldsymbol{x}}$ is the third-order tensor of derivatives of the potential energy. In what follows we assume that the scale of characteristic fluctuations of the coordinates is set by the equipartition theorem, namely $\langle x^2\rangle\sim k_BT$, and therefore higher order products of coordinates are much smaller than k_BT. With this assumption, we expand the numerator of Eq. (B.1) as

$$\begin{aligned}\int\mathcal{A}(\boldsymbol{x})\exp\left(-\frac{\delta\mathcal{U}(\boldsymbol{x})}{k_BT}\right)d\boldsymbol{x}&\simeq\int\left(\mathcal{A}_0+\frac{\partial\mathcal{A}}{\partial\boldsymbol{x}}\cdot\boldsymbol{x}+\frac{1}{2}\frac{\partial^2\mathcal{A}}{\partial\boldsymbol{x}\partial\boldsymbol{x}}:\boldsymbol{x}\boldsymbol{x}\right)\exp\left(-\frac{\boldsymbol{\mathcal{M}}:\boldsymbol{x}\boldsymbol{x}}{2k_BT}\right)\left(1-\frac{\boldsymbol{\mathcal{U}}'''\vdots\boldsymbol{x}\boldsymbol{x}\boldsymbol{x}}{6k_BT}\right)d\boldsymbol{x}\\&\simeq\int\left(\mathcal{A}_0+\frac{1}{2}\frac{\partial^2\mathcal{A}}{\partial\boldsymbol{x}\partial\boldsymbol{x}}:\boldsymbol{x}\boldsymbol{x}-\frac{1}{6k_BT}\boldsymbol{x}\cdot\frac{\partial\mathcal{A}}{\partial\boldsymbol{x}}\boldsymbol{\mathcal{U}}'''\vdots\boldsymbol{x}\boldsymbol{x}\boldsymbol{x}\right)\exp\left(-\frac{\boldsymbol{\mathcal{M}}:\boldsymbol{x}\boldsymbol{x}}{2k_BT}\right)d\boldsymbol{x}\\&=\left(\mathcal{A}_0+\frac{k_BT}{2}\left[\frac{\partial^2\mathcal{A}}{\partial\boldsymbol{x}\partial\boldsymbol{x}}:\boldsymbol{\mathcal{M}}^{-1}-\frac{\partial\mathcal{A}}{\partial\boldsymbol{x}}\cdot\boldsymbol{\mathcal{M}}^{-1}\cdot\boldsymbol{\mathcal{U}}'''\vdots\boldsymbol{\mathcal{M}}^{-1}\right]\right)\int\exp\left(-\frac{\boldsymbol{\mathcal{M}}:\boldsymbol{x}\boldsymbol{x}}{2k_BT}\right)d\boldsymbol{x}\,,\end{aligned} \tag{B.3}$$

where we have used the identities

$$\int\boldsymbol{x}_i\boldsymbol{x}_j\exp\left(-\frac{\boldsymbol{\mathcal{M}}:\boldsymbol{x}\boldsymbol{x}}{2k_BT}\right)d\boldsymbol{x}=T\boldsymbol{\mathcal{M}}^{-1}_{ij}\int\exp\left(-\frac{\boldsymbol{\mathcal{M}}:\boldsymbol{x}\boldsymbol{x}}{2k_BT}\right)d\boldsymbol{x}\,,$$

$$\int\boldsymbol{x}_i\boldsymbol{x}_j\boldsymbol{x}_k\boldsymbol{x}_m\exp\left(-\frac{\boldsymbol{\mathcal{M}}:\boldsymbol{x}\boldsymbol{x}}{2k_BT}\right)d\boldsymbol{x}=T^2\left(\boldsymbol{\mathcal{M}}^{-1}_{ij}\boldsymbol{\mathcal{M}}^{-1}_{km}+\boldsymbol{\mathcal{M}}^{-1}_{ik}\boldsymbol{\mathcal{M}}^{-1}_{jm}+\boldsymbol{\mathcal{M}}^{-1}_{im}\boldsymbol{\mathcal{M}}^{-1}_{jk}\right)\int\exp\left(-\frac{\boldsymbol{\mathcal{M}}:\boldsymbol{x}\boldsymbol{x}}{2k_BT}\right)d\boldsymbol{x}\,.$$

Since $\tilde{\mathcal{Z}}(T)\simeq\left(1+\mathcal{O}(k_BT)\right)\int\exp\left(-\frac{\boldsymbol{\mathcal{M}}:\boldsymbol{x}\boldsymbol{x}}{2k_BT}\right)d\boldsymbol{x}$, we arrive at the result

$$\frac{\langle\mathcal{A}\rangle_{_T}-\mathcal{A}^{(0)}}{\frac{1}{2}k_BT}\simeq\frac{\partial^2\mathcal{A}}{\partial\boldsymbol{x}\partial\boldsymbol{x}}:\boldsymbol{\mathcal{M}}^{-1}-\frac{\partial\mathcal{A}}{\partial\boldsymbol{x}}\cdot\boldsymbol{\mathcal{M}}^{-1}\cdot\boldsymbol{\mathcal{U}}'''\vdots\boldsymbol{\mathcal{M}}^{-1}\,. \tag{B.4}$$

as appears in the main text. We stress that the effect of higher order derivatives of both $\mathcal{A}$ and $\mathcal{U}$ can also be explicitly calculated and is of a higher order in T (not shown).

In this work we study the local thermal energy (LTE), defined as follows: we focus on potential energy functions that can be written as a sum over pairwise interactions $\mathcal{U}=\sum_\alpha\varepsilon_\alpha$, where α labels the different pairs of interacting degrees of freedom. Using Eq. (B.4), we define the local thermal energy $\mathcal{E}_\alpha$ as

$$\begin{aligned}\mathcal{E}_\alpha&\equiv\lim_{T\to0}\frac{\langle\varepsilon_\alpha\rangle_{_T}-\varepsilon_\alpha^{(0)}}{\frac{1}{2}k_BT}\\&=\frac{\partial^2\varepsilon_\alpha}{\partial\boldsymbol{x}\partial\boldsymbol{x}}:\boldsymbol{\mathcal{M}}^{-1}-\frac{\partial\varepsilon_\alpha}{\partial\boldsymbol{x}}\cdot\boldsymbol{\mathcal{M}}^{-1}\cdot\boldsymbol{\mathcal{U}}'''\vdots\boldsymbol{\mathcal{M}}^{-1}\,.\end{aligned} \tag{B.5}$$

Examples of the LTE fields calculated in 2D model glasses can be found in Figs. 1 and 3 in the main text. These fields are calculated as follows: we perform a full diagonalization of the dynamical matrix $\boldsymbol{\mathcal{M}}$ calculated for each glassy sample, and obtain the complete set of eigenmodes $\{\boldsymbol{\Psi}_\ell\}_{\ell=1}^{N\hat{d}}$ and their associated eigenfrequencies $\{\omega_\ell\}_{\ell=1}^{N\hat{d}}$, where $\hat{d}$ is the spatial dimension. We then

solve the following linear equation for the thermal displacements $\boldsymbol{\mathcal{X}} \equiv -\boldsymbol{\mathcal{M}}^{-1}\cdot\boldsymbol{\mathcal{U}}''' : \boldsymbol{\mathcal{M}}^{-1}$ (see main text) using a conventional conjugate gradient solver

$$\boldsymbol{\mathcal{M}}\cdot\boldsymbol{\mathcal{X}} = -\sum_{\ell} \frac{\boldsymbol{\mathcal{U}}''' : \boldsymbol{\Psi}_\ell \boldsymbol{\Psi}_\ell}{\omega_\ell^2} \tag{B.6}$$

Expressions for $\boldsymbol{\mathcal{M}}$ and $\boldsymbol{\mathcal{U}}'''$ for pairwise potentials are available in e.g. [5]. Finally, the LTE $\mathcal{E}_\alpha$ is calculated for each interaction α as

$$\mathcal{E}_\alpha = \sum_{\ell} \frac{\frac{\partial^2 \varepsilon_\alpha}{\partial \boldsymbol{x}\partial \boldsymbol{x}} : \boldsymbol{\Psi}_\ell \boldsymbol{\Psi}_\ell}{\omega_\ell^2} + \frac{\partial \varepsilon_\alpha}{\partial \boldsymbol{x}} \cdot \boldsymbol{\mathcal{X}} \,. \tag{B.7}$$

The formalism presented above remains valid for systems in which the potential is written as a sum of 3-body (or higher) terms, e.g. [6]. In this case $\mathcal{U} = \sum_\alpha \varepsilon_\alpha$, where now α labels a *triple* of interacting particles. The same expression given in Eq. (B.5) would now describe the LTE associated with the triple α. A key point is that the forces

$$\boldsymbol{f}_\alpha \equiv \frac{\partial \varepsilon_\alpha}{\partial \boldsymbol{x}} \tag{B.8}$$

have a different form in the case of 3-body interactions compared to the case of pairwise interactions. In the latter, if the interaction is radially-symmetric, $\boldsymbol{f}_\alpha$ has the geometry of a dipole vector acting on the pair α, as illustrated in the left panel of Fig. 1. What is the form of $\boldsymbol{f}_\alpha$ for 3-body interactions? As an example, assume that the interaction $\varepsilon_\alpha = \varepsilon_\alpha(\theta_\alpha)$ depends upon the angle θ_α formed between a triple i, j, k of particles. In this case, $\boldsymbol{f}_\alpha$ is a field with the geometry as illustrated in the right panel of Fig. 1.

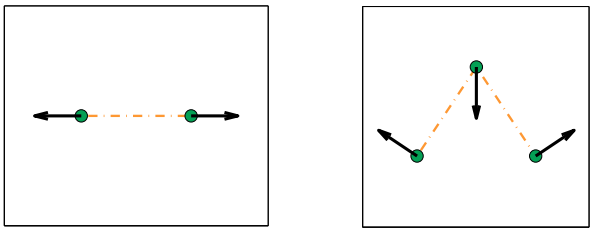

FIG. 1. Left panel: the geometry of $\boldsymbol{f}_\alpha$ in the case that ε_α is a pairwise radially-symmetric interaction. Right panel: same as left panel, for the case of a 3-body ε_α which depends on the angle between the triple of nodes.

We assert that as long as the interaction potential is translationally and rotationally invariant (i.e. it only depends on the relative distances and orientations between the triple α), the associated $\boldsymbol{f}_\alpha$ will be of a form which, when contracted with a slowly-varying field in space, will pick up contributions that are proportional to the spatial gradient of the slowly-varying field. The same reasoning also applies to contractions of slowly-varying fields with the third-order tensor $\boldsymbol{\mathcal{U}}'''$ as well. For these reasons, we expect LTEs to always filter out collective translational modes, and therefore be insensitive to the presence of low-frequency plane-waves, independently of the particular form of the potential energy.

Finally, we comment on the computational complexity of our numerical analysis: the bottleneck of the calculation is the requirement to obtain all the eigenmodes and eigenvalues of the dynamical matrix. The computational time of this full-diagonalization is known to scale as N^3. The computational time dedicated to the rest of the analysis is negligible compared to the diagonalization step. It is left for future research to investigate whether a partial diagonalization of the dynamical matrix (which would simply result in truncated sums in Eqs. (B.6) and (B.7)) would suffice for producing softness maps with comparable predictive powers to those obtained using a full diagonalization.

C. DISTRIBUTION OF FORCE MAGNITUDES

In the main text we present a scaling argument according to which the distribution of LTEs should follow $p(\mathcal{E}_\alpha) \sim \mathcal{E}_\alpha^{-9/4}$, based on the recent discovery that the asymptotic form of the distribution of glassy low-frequency modes in glassy systems follows $D_G(\omega) \sim \omega^4$ [7]. In this argument, we assume that the magnitudes of forces between the glass particles is narrowly distributed. Here, we present numerical evidence that validates this assumption: in Fig. 2 we present the distribution of the magnitude of pairwise forces between particles in the 3DIPL system, showing that it decays superexponentially at large values.

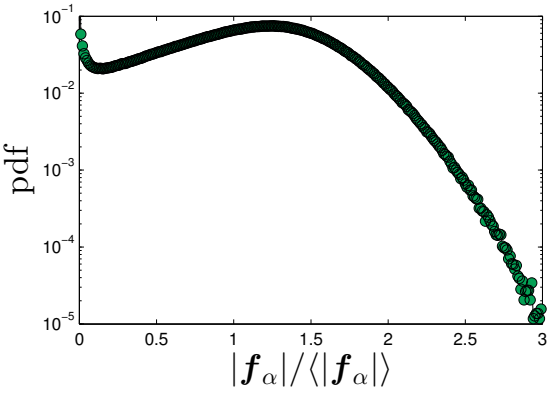

FIG. 2. The distribution of the magnitude of forces between particles measured for the 3DIPL system shows a superexponential decay at large values.

D. IDENTIFYING SOFT SPOTS AND THEIR DEGREE OF SOFTNESS

To quantitatively analyze the heterogenous spatial distribution of LTE $\mathcal{E}_\alpha$, we construct coarse-grained 2D map as follows. Space is discretized into bins of the smallest size which proved to always include at least two bonds' center of masses. In our case, it corresponds to a bin size of $1/40L$, with L being the linear size of the simulation box. The coarse-grained map is then built in two steps. In the first step, each bond is associated with a bin selected according to the bond's center of mass and the absolute value of its LTE contributes to the bin's value. In the second step, the map is smoothed out by averaging the bin's value with the values of all bins in the first layer of neighboring bins (8 bins in 2D). For easier processing, bonds with an associated LTE value smaller than $|\mathcal{E}_\alpha|=1.1$ were omitted. We verified that this choice does not affect the results, which are sensitive to large values of $|\mathcal{E}_\alpha|$.

The local maxima of the coarse-grained map were then extracted. These maxima are identified with soft spots, as described next. We first analyzed each row of the 2D maps at a time, where the bins corresponding to a local maximum were flagged. We repeated the same flagging procedure for every column. Bins which were flagged twice were defined as soft spots. As the exact location of the soft spot within the bin's area is of no interest, we define the soft spot location as the bin's coordinate with added white noise to avoid discretization effects. We used the bin's value as the soft spot score $\hat{\eta}$, which describes the average value of $|\mathcal{E}_\alpha|$ in the near vicinity of the soft spot center.

The LTE of bonds are widely distributed and consequently so are the scores of the soft spots, both within and between realizations. We therefore adopt the following standardized score

$$\Delta_{\mathcal{E}} = \frac{\eta_{\max}}{\hat{\eta}_i} \ , \tag{E.1}$$

where $\hat{\eta}_i$ is the score of the i^{th} soft spot and $\eta_{\max} = \max_i [\hat{\eta}_i]$ evaluated for each realization. Therefore, the softest spot in each realization has $\Delta_{\mathcal{E}}=1$ and not-as-soft spots are characterized by $\Delta_{\mathcal{E}}>1$, where the deviation from unity quantifies the degree of softness within each realization. This standardization allows a consistent numerical analysis per realization, as well as the calculation of distribution functions based on a large number of realizations. The analysis is based on 5000 independent realizations, where a few tens of soft spots were detected per realization. Among these spots, the softest ones — i.e. those with $\Delta_{\mathcal{E}}$ close to unity — dominate the plastic response under shearing. For example, there are on average 25 spots with $\Delta_{\mathcal{E}}\leq 2$, which according to Fig. 4 (left), predict nearly 70% of the first plastic events.

E. QUANTIFYING PREDICTIVENESS OF PLASTIC REARRANGEMENTS UNDER SHEAR

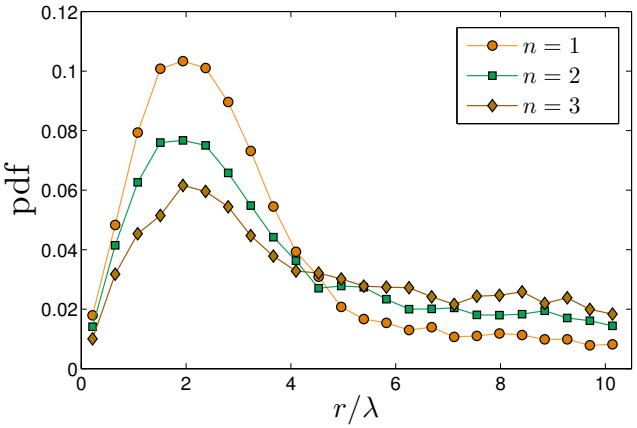

FIG. 3. The probability distribution function of the distance r (normalized by the bond-length between two small particles λ, cf. Eq. (A.1) and the text below it) between plastic events and the center of the nearest soft spot. It is observed that plastic events occur with high-probability close — within a few bond-lengths — to soft spots.

Plastic rearrangements — The performed athermal quasi-static shearing simulations followed well-established two-step protocols of first imposing an affine simple-shear transformation to the system and then minimizing its energy while enforcing Lees-Edwards boundary conditions, see e.g. [8–10]. During these simulations the energy was used as an indicator of plastic rearrangements/events which were identified with strain precision up to 10^{-6} using backtracking methods. The plastic events were automatically spatially localized by selecting the particle with the largest displacement value as a consequence of the energy minimization step at the occurrence of the plastic event.

Quantification — Each glass realization was sheared until 5 plastic events were triggered. The probability distribution function of the distance of plastic events to the nearest spot in space is shown in Fig. 3. It is observed that plastic events occur with high-probability near soft spots (corresponding to the peak around 2 bond-lengths). Consequently, we identify the soft spot which is closest to the k^{th} plastic event and record its standardized score $\Delta_{\mathcal{E}}$ for further analysis as described in the manuscript.

Normal-modes maps — To compare the LTE results with existing methods/results in the literature, we followed the protocol described in [11] to produce a field which is based on the 30 lowest normal-modes with non-vanishing associated energy. By constructing such normal-modes-based maps, each and every particle in the system has a score corresponding to a sum over the displacement squared of the modes. We then applied exactly the same protocol described in Section **D** in the context

of the LTE maps to the normal-modes-based maps, where bonds' centers of mass were replaced with particle positions and the LTE absolute values of bonds were replaced with particles' scores. The results of the comparison are presented in the main text.

[1] Bailey NP, Pedersen UR, Gnan N, Schrder TB, Dyre JC (2008) Pressure-energy correlations in liquids. i. results from computer simulations. *J. Chem. Phys.* 129(18):184507.

[2] Dyre JC (2016) Simple liquids quasiuniversality and the hard-sphere paradigm. *Journal of Physics: Condensed Matter* 28(32):323001.

[3] Bacher AK, Schrøder TB, Dyre JC (2014) Explaining why simple liquids are quasi-universal. *Nat. Commun.* 5.

[4] Kob W, Andersen HC (1995) Testing mode-coupling theory for a supercooled binary lennard-jones mixture i: The van hove correlation function. *Phys. Rev. E* 51(5):4626–4641.

[5] Karmakar S, Lerner E, Procaccia I (2010) Athermal nonlinear elastic constants of amorphous solids. *Phys. Rev. E* 82(2):026105.

[6] Stillinger FH, Weber TA (1985) Computer simulation of local order in condensed phases of silicon. *Phys. Rev. B* 31(8):5262–5271.

[7] Lerner E, Düring G, Bouchbinder E (2016) Statistics and properties of low-frequency vibrational modes in structural glasses. *Phys. Rev. Lett.* 117(3):035501.

[8] Maloney C, Lemaître A (2004) Subextensive scaling in the athermal, quasistatic limit of amorphous matter in plastic shear flow. *Phys. Rev. Lett.* 93(1):016001.

[9] Maloney CE, Lemaître A (2006) Amorphous systems in athermal, quasistatic shear. *Phys. Rev. E* 74(1):016118.

[10] Karmakar S, Lerner E, Procaccia I, Zylberg J (2010) Statistical physics of elastoplastic steady states in amorphous solids: Finite temperatures and strain rates. *Phys. Rev. E* 82(3):031301.

[11] Widmer-Cooper A, Perry H, Harrowell P, Reichman DR (2008) Irreversible reorganization in a supercooled liquid originates from localized soft modes. *Nature Phys.* 4(9):711–715.